High-resolution PIV analysis of compressibility effects in turbulent jets

G. Ceglia[1], D. Violato[2], M. Tuinstra[3] and F. Scarano[2]

[1] DII, Dipartimento di Ingegneria Industriale, Università degli Studi di Napoli Federico II, P.le Tecchio 80, 80125 Napoli, Italy
giuseppe.ceglia@unina.it

[2] Aerospace Engineering Department, Delft University of Technology, Kluyverweg,1, 2629 HS, Delft, The Netherlands

[3] National Aerospace Laboratory, Voorsterweg 31, 8316 PR Marknesse, The Netherlands

ABSTRACT

An investigation on the compressibility effects arising into the near field of turbulent jets operated at high Reynolds number at Mach numbers M=0.3, 0.9 and 1.1 (under-expanded regime) is carried out with two-components planar PIV experiments with high resolution cameras. The arrangement of the PIV system allows for mapping out the flow field with a vector pitch equal to 0.17mm along the streamwise direction. The flow field is characterized by single-point statistics. For the under-expanded jet, the spatial evolution of the flow field within the potential core region is characterized by the presence of shock-cell structures that extend up to 4.5 D downstream from the nozzle exit.
Two-point cross-correlation technique is used to investigate the large scale coherent structures in the potential core and in the shear layer. The distribution of the longitudinal spatial correlations valuated in the potential core region of the jet exhibits a phase shifted pattern in sign that extends periodically along the jet axis. This spatial phase shift is approximately 0.5 D for M=0.3 and 0.25 D for M=1.1. Downstream from x/D=2 and r/D=0, the intensity of the peaks of the spatial correlations in the underexpanded jet is higher than that calculated at Mach 0.3 jet because of the presence of the shock-cell structures in the potential core.

INTRODUCTION

The turbulent structures of jets at high Reynolds numbers have been largely investigated in relation to several engineering applications [1], but also in the framework of fundamental studies on turbulence [2]. In presence of compressibility effects, the large-scale flow structures become more complex than in incompressible flows. In particular with increasing of the compressibility the flow exhibits a more complex three-dimensional organization. Experimental studies describing the large-scale patterns arising from the near field are thus relevant to understand the influence of the compressibility on the organization of the turbulent structures.
The evolution of coherent structures arising in the near field of a round jet at different Reynolds numbers ranging from order 10^2 to 10^5 was firstly studied by [3], who recognized large-scale structures in the jet shear layer that become less organized as the Reynolds number increases. Using a conditional sampling technique, Yule [4] identified different vortical structures arising in the transitional region of a round jet using flow visualization technique and hot-wire measurements. The interaction and coalescence of the vortex rings in the transition region and the subsequent formation of large eddies in the turbulent region was described. Further investigations reviewed by [5] pointed out the mechanism of vortex interaction as azimuthal vortex pairing that occurs in two distinct instability modes [6], shear layer mode and jet column mode, based on momentum thickness and jet diameter length-scales, respectively. A high strain braid region occurring between consecutive vortex rings is influenced by the evolution of counter rotating streamwise vortex pairs leading to the flow transition to turbulence [7]. Using planar Particle Image Velocimetry (PIV) [8] and LIF visualizations, Liepmann and Gharib [7] showed how streamwise vortex pairs promote the growth of the jet and the amplification of the shear layer instabilities due to the entrainment process.
The role of the compressibility in the formation and development of the large-scale structures was experimentally studied in planar shear layers [9-10] and jets [11-12]. Brown and Roshko [9] investigated two

streams of different gases issuing at Reynolds number of the order of 10^6. With flow visualization technique, they showed the presence of large coherent structures that dominate the mixing layer leading to a concept that the turbulence characteristics are strongly influenced by compressible effects. In subsequent measurements, Papamoschou and Roshko [11] introduced a non-dimensional parameter, the convective Mach number, in order to categorize and evaluate the degree of the compressibility. Murakami and Papamoschou [12] performed an experimental investigation on the morphology and evolution of large turbulent eddies in a ideally expanded supersonic jet at Mach M=1.5. They carried out that the convective velocity of coherent structures in the shear layer indicates different compressible regimes. Further experiments using time resolved flow visualization performed by Thurow et al. [13] show the evolution of coherent structures that evolve in the shear layer of Mach M=1.3 and 2.0 ideally expanded high Reynolds number axisymmetric jets. They generalized and decomposed the evolution of the coherent structures under the action of the compressible effects into the basic processes of tilt, stretch, tear and pair. As the Mach number increases, these events occur more frequently and the coherent structures become less coherent and distinct with respect to the rest of the shear layer. Combining different measurements techniques, Hileman et al. [14] analyzed the evolution of coherent structures within an ideally expanded Mach M=1.28 high Reynolds number jet. Using Proper Orthogonal Decomposition technique (POD, [15]), in correspondence of high and low sound emission events they recognized large scale fluid modes associated with the acoustic features of the evolving jet.

In a Mach 0.85 jet, Seiner et al. [16] estimated and subsequently analyzed two-point spatial correlations which are known to be relevant to source terms of Lighthill turbulent stress tensor [17]. The authors highlighted also the requirement to extend the actual investigation to 3-D field correlated in time with an adequate sampling rate. Two-point turbulence statistics were also reported by Ukeiley et al. [18] and by Tinney et al [19] for a turbulent jet in the same exit conditions. They found the presence of helical coherent structures in the shear layer at x/D=4 and 8. Using dual-plane PIV measurements, Fleury et al. [20] estimated space-time correlations in a subsonic jet at Mach 0.6 and 0.9. Self-similarity of spatial correlation turbulent statistics was found in the shear layer and on the jet axis. Using single and multi-point laser Doppler velocimetry measurements performed in a Mach 1.2 cold supersonic jet, Kerhervé et al. [21] pointed out that the axial evolution of the integral scales based on the fourth-order and second-order correlations are similar to that found in subsonic flow, although the scales are globally smaller.

The objective of this investigation is to characterize the coherent structures present in the near field of high-speed turbulent jet operated at high Reynolds number up to transonic regime at Mach number M=0.3, 0.9 and 1.1. The difficulties in the use of hot-wire at high velocities in correspondence with high Reynolds number motivated to perform a set of planar PIV measurements. High spatial resolution planar PIV experiments are performed in order to determine to what extent the compressibility effects on the large-scale structures arising within the first 8 diameters of the investigated jets. Axial mean velocity profiles from PIV realizations are shown in form of similarity variables [22] and two-point turbulent correlations of axial-radial components calculated from planar PIV measurements for Mach 0.3 and 1.1 jets are calculated in order to investigate on how two-point correlation distributions are influenced by compressible effects increase as well as with the presence of shock-cell structures in the potential core for the under-expanded regime.

EXPERIMENTAL APPARATUS

JET FLOW FACILITY

The experiments are conducted at the Aerodynamic Laboratories of the Aerospace Engineering Department at TU Delft. A contoured axisymmetric shaped nozzle of exit diameter D=22mm and contraction ratio 4.4:1 is installed on the bottom wall of the Jet Tomography Facility (JTF) developed in previous works [23]. Stabilized air supply of 0.18kg/s is provided upstream of the contraction in the settling chamber with the use of a choking plate with constant nominal diameter of 100mm at a pressure of approximately of 3bar.

Measurements are performed at Mach 0.3, 0.9 and 1.1. The exit velocity U_j are, respectively, 105m/s, 282m/s and 327m/s, corresponding to Reynolds numbers of $150 \cdot 10^3$, $380 \cdot 10^3$ and $460 \cdot 10^3$ based on the jet diameter D.

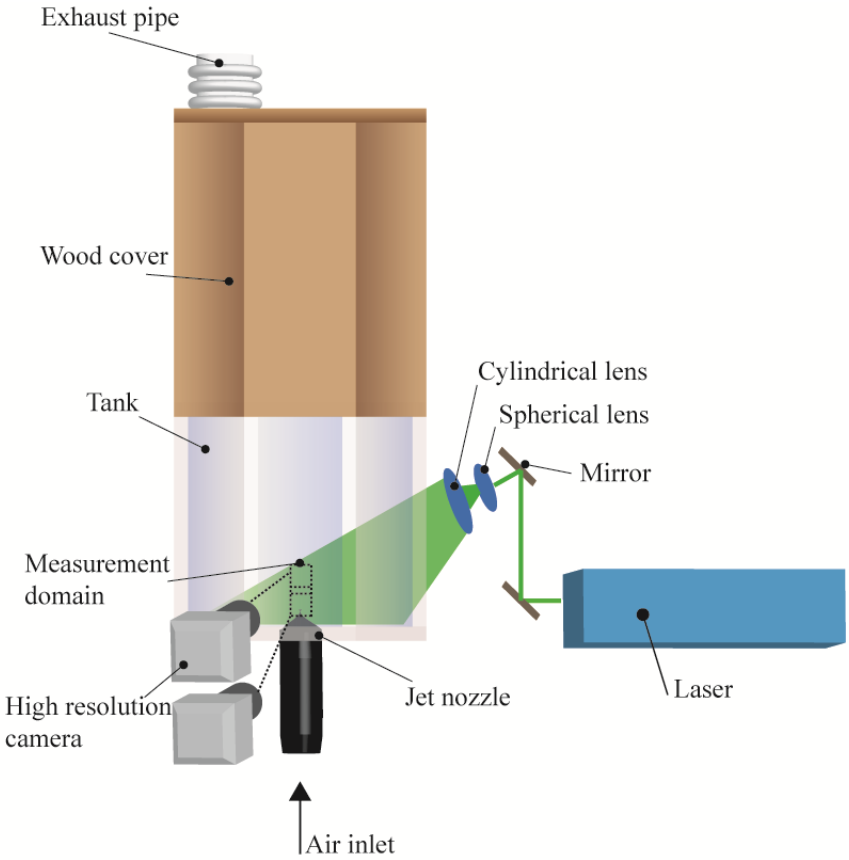

Figure 1 Schematic view of the illumination and imaging settings of the experiments.

PLANAR PIV MEASUREMENTS

The flow is seeded with DEHS particles of 1μm median diameter and the flow in the jet and in the surrounding space is seeded with a concentration of about 100particles/mm^3.
Two-dimensional velocity field measurements are conducted with planar two-component PIV (2C-2D PIV). Laser pulses are produced with a double-cavity Spectra-Physics Quanta Ray Nd:YAG system (532 nm, 400mJ/pulse, 6 ns pulse duration).
The exit beam of 7mm diameter is shaped into a light sheet of 1.5mm thickness by the combination of 2 spherical lenses with -100mm and 100mm focal length and of a cylindrical lens with -60mm focal length. The illumination set-up is sketched in Fig.1. Although the modified configuration of the JTF provides a height of approximately 100 jet diameters.
The requirement to capture the processes occurring at the jet core breakdown set the field of view (FOV) to about 8.2 D along the jet axis, corresponding to approximately 180mm. This is achieved by the simultaneous use of 2 LaVision Imager Pro LX 16M cameras (4872x3248 pixels, pixel pitch 7.4μm) arranged along the streamwise direction. The resulting digital resolution was of 47pixels/mm. The FOV of each camera is 3.2 x 4.7 D^2 (70mm x 104mm) with an overlap between cameras FOVs of 0,6 D (13mm). After combining the two velocity fields, the total measurement domain is of 3.2 x 8.9 D^2 (70mm x 195mm).
The synchronization between the illumination and the image acquisition systems as well as the image analysis are performed by means of a LaVision Programmable Timing Unit 9 connected to a workstation running the *Lavision* software DaVis 8.
The experiments were performed in series of 500 recordings at a measurement rate of 0.8Hz.
The images interrogation is performed by a multi-pass cross-correlation with a multi-grid technique with final window size of 32 x 32 pixels (0.7 x 0.7 mm^2) and 75% overlap factor, yielding a vector pitch of 0.17mm. The resulting measurement grid counts approximately a half million vectors at each snapshot (420 x 1150 vectors). The image background intensity is attenuated by minimum pixel intensity subtraction over the whole sequence. The details of the experimental settings are summarized in Table 1.

Seeding	diameter [μm] concentration [particles/mm^3]	1 86.7
Illumination	Spectra-Physics *Quanta Ray* double cavity Nd:Yag laser (2 x 400mJ@10Hz)	sheet thickness 1.5 mm
Recording device	LaVision Imager Pro LX 16M cameras (4872x3248 pixels@ 3Hz)	2 cameras
Optical arrangement	Nikon objectives (f ; f#) field of view	105mm; 4 3.2D x 9.5D
Magnification		0.35
Acquisition frequency		0.8Hz
Pulse separation: M=0.3, M=0.9 M=1.1		 3μs 1μs 1μs
Number of recordings		500

Table 1 Experimental parameters.

RESULTS AND DISCUSSION

STATISTICAL ANALYSIS

The global information on the turbulent structures of the jet in incompressible regime and under the compressibility effects are evaluated in terms of the mean and turbulence statistics. In this section the axial $U(x,r,t)$ and radial $V(x,r,t)$ component of the velocity field are decomposed into a temporal average part $\overline{U(x,r,t)}$ and $\overline{V(x,r,t)}$ (the overbar indicates the operation of time-averaging) and a fluctuating part $u'(x,r,t)$ and $v'(x,r,t)$. Where x, r and t are the axial, radial and time coordinates, respectively.

In Fig. 2, the iso-contour of the axial mean velocity component $\overline{U}$ for Mach numbers M=0.3 and 1.1 are shown with the velocity profiles along the radial direction at several axial positions. The spatial evolution of the jets shown in Fig. 2a highlights the presence of the potential core region characterized by the constant velocity value equal to 105m/s. In Fig. 2b, a detailed inspection of the velocity map for under-expanded regime reveals the presence of shock-cell structures into the potential core region. The peak of the mean axial velocity about of 359m/s is reached at x/D=0.2.

The iso-contour of the root mean square (rms) of the axial velocity fluctuation $\sqrt{\overline{u'u'}}/U_j$ normalized by the jet exit velocity at M=0.3 and M=1.1 are depicted in Fig. 3. The turbulent intensity distribution shows a maximum value about of 16% and 18% for M=0.3 and 1.1, respectively, in agreement with the results reported by [23] and [27]. An interesting feature is the presence of the peaks of the rms of the axial velocity fluctuation along the centreline of the jet into the potential core region for the under-expanded regime (Fig. 3b). The local maximum values of the $\sqrt{\overline{u'u'}}/U_j$ and the $\overline{U}/U_j$ per each shock-cell are reached at same axial positions x/D. Further downstream, the intensity of the $\overline{U}/U_j$ decreases, whereas the peaks of the $\sqrt{\overline{u'u'}}/U_j$ are less pronounced and more intense.

The distribution of the normalized mean axial velocity $\overline{U}/U_j$ and the normalized rms of the axial velocity fluctuation $\sqrt{\overline{u'u'}}/U_j$ along the centreline for Mach numbers M=0.3, 0.9 and 1.1 are shown in Fig. 4a and b, respectively. As expected, for M=0.3 and 0.9 the distributions of the mean axial velocity component are nearly constant with respect to the axial direction within the initial region of the jet. In agreement with the results reported by [28], the length of the potential core L_c is about 5 D for M=0.3, whereas for M=0.9 L_c is about 6 D according to [23] and [24]. For Mach 1.1, the axial mean velocity is normalized with the average value of the mean axial velocity profile along the centreline between $x/D = 1$ and 3. In the under-expanded regime, the distributions of the mean and turbulence velocity ratios exhibit a sinusoidal pattern with a wave length equal to 0.46 D within the initial region of the jet. This behavior is due to the presence of the shock-cells structures that extend up to 4.5 D downstream from the nozzle exit.

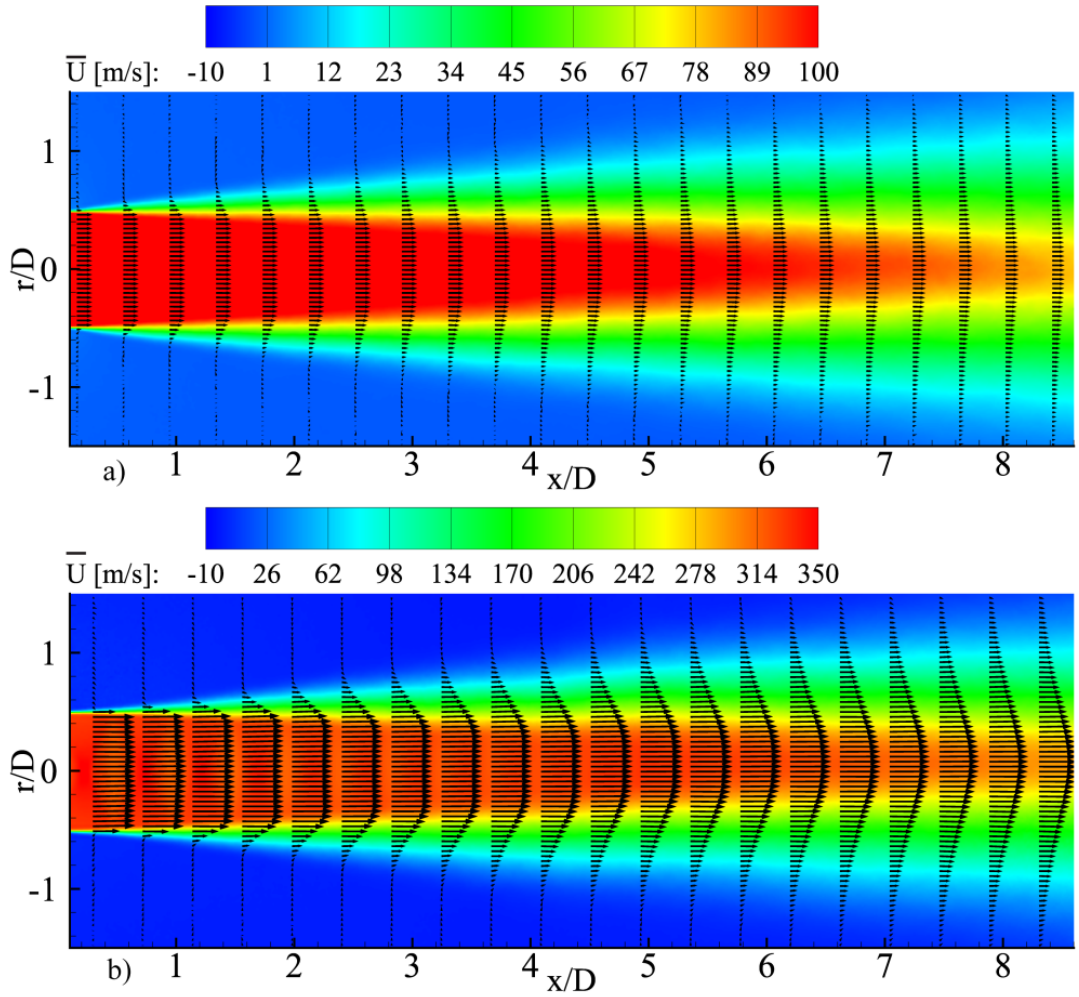

Figure 2 Iso-contours of mean axial velocity maps $\overline{U}/U_j$ at Mach M=0.3 (a) and M=1.1 (b). Velocity profiles are placed each 50 and 5 measured vectors along axial and radial directions, respectively.

In Fig. 4b, the jet's transitional regions are reached more rapidly for Mach 0.3 when compared to the transonic and under-expanded jets (Mach 0.9 and 1.1, respectively).

The radial profiles of the normalized mean axial velocity $\overline{U}/U_j$ and the normalized rms of the axial $\sqrt{\overline{u'u'}}/U_j$ and radial $\sqrt{\overline{v'v'}}/U_j$ turbulent fluctuations are shown in Fig. 5 between x/D=1 and 6 for M=0.3, 0.9 and 1.1. The profiles of the mean and turbulence statistics are obtained using the similarity variable $\eta = (r - r_{0.5})/\delta$, where r is the radial coordinate, $r_{0.5}$ is the radial location where the mean axial velocity is 50% of the U_j and δ is the shear-layer thickness defined as $\delta = (r_{0.9} - r_{0.1})$, with $r_{0.9}$ and $r_{0.1}$ being the radial locations at $\overline{U}/U_j$=0.9 and 0.1, respectively. Within the initial region of the jets, the development of the flow follows a self-similar trend and the collapse is consistent with the studies on high subsonic jets reported by [19-20-24-25]. In Fig. 5a, the presence of the shock-cells structures lead to a displaced values of the $\overline{U}/U_j$ profiles slightly below the unity near the jet axis as reported by [21].

Fig. 6 shows the distribution of the normalized shear layer thickness with respect to the centreline of the jet for Mach numbers M=0.3, 0.9 and 1.1. As expected the shear layer width is reduced when the Mach number increases.

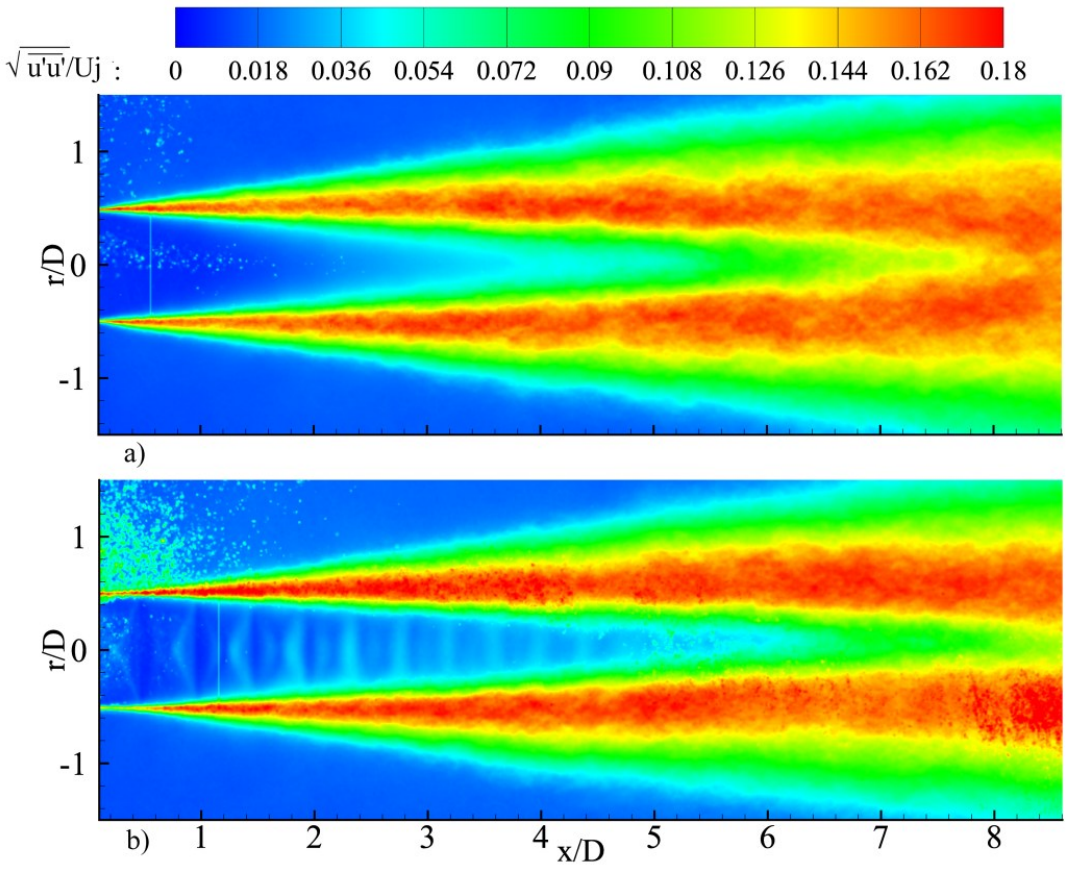

Figure 3 Iso-contours of the axial velocity fluctuation maps $\sqrt{\overline{u'u'}}/U_j$ at Mach M=0.3 (a) and 1.1 (b).

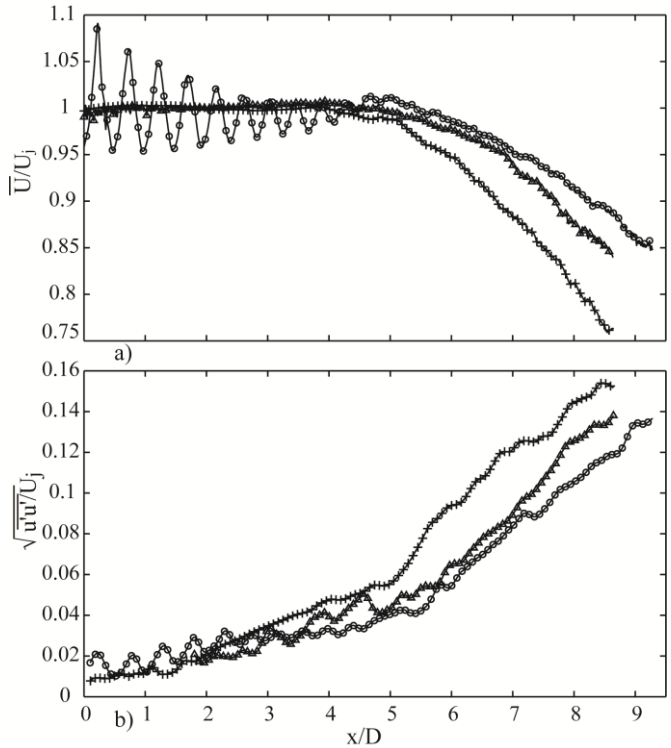

Figure 4 Centerline distribution of (a) normalized mean axial velocity $\overline{U}/U_j$ and (b) normalized rms of the axial velocity fluctuations $\sqrt{\overline{u'u'}}/U_j$ at Mach M=0.3 (+), 0.9 (△), 1.1 (○). Symbols are placed each 10 measured vectors.

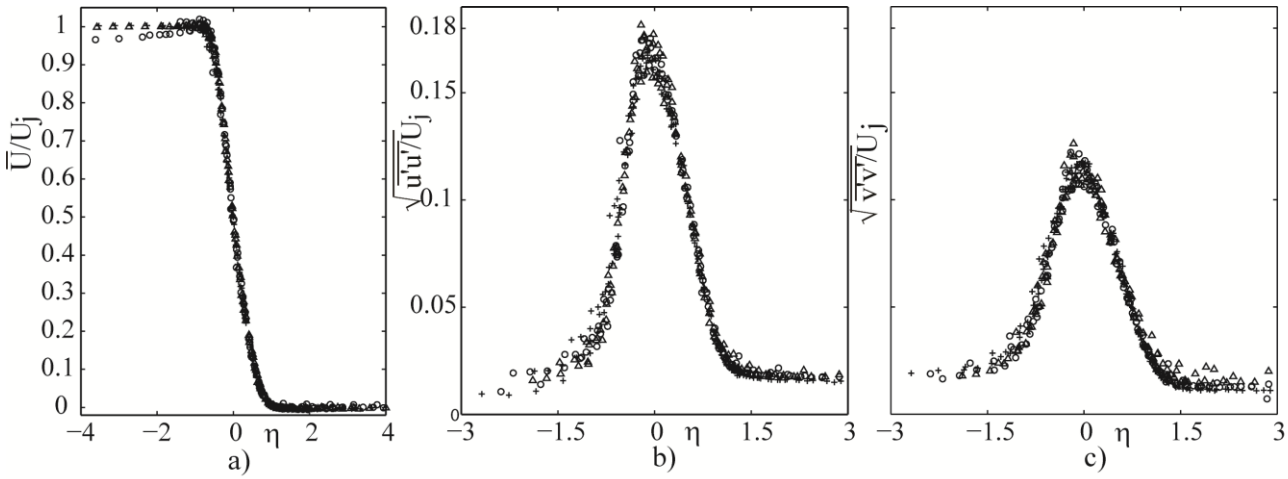

Figure5 Radial distribution of (a) normalized axial mean velocity profiles U/U_j, (b) normalized rms of turbulent axial $\sqrt{\overline{u'u'}}/U_j$ and (c) radial $\sqrt{\overline{v'v'}}/U_j$ fluctuations in the shear layer from x/D=1 to x/D=6 every $\Delta x/D$=1 at Mach M=0.3 (+), 0.9 (△), 1.1 (○). Symbols are placed each 8 measured vectors.

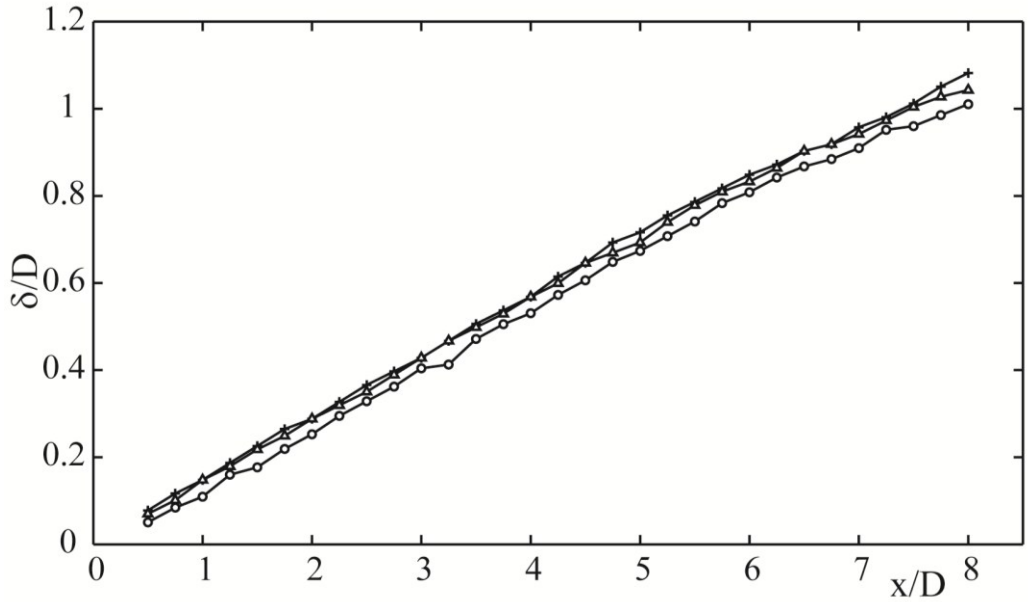

Figure 6 Distribution of the normalized shear layer thickness δ/D along the centreline for Mach numbers M=0.3 (+), 0.9 (△), 1.1 (○).

TWO-POINT STATISTICS

The two-point correlations are evaluated across the jet streamwise and radial plane (x-r). the normalized correlations is defined as follows:

$$R_{ij}(x,r) = \frac{\overline{u'_i(x,r,t)\,u'_j(x_0,r_0,t)}}{\left(\overline{u'_i(x,r,t)^2}\right)^{0.5}\left(\overline{u'_j(x_0,r_0,t)^2}\right)^{0.5}} \qquad (1)$$

The coordinates of the origin of the spatial correlations are indicated with x_0 and r_0 and are fixed at two radial locations r/D=0 and 0.5 (in the shear layer region of the jet) and two axial positions x/D=2 and 7.
The longitudinal and transversal correlations valuated at r/D=0 and x/D=2 for Mach numbers M=0.3 and 1.1 are shown in Figs. 7 and 8, respectively. A more interesting feature is the distribution of the longitudinal correlations in the potential core region of the jet. In particular for M=0.3 (Fig. 7a), the correlation map exhibits a spatial phase shift in sign of approximately 0.5 D. Downstream from the fixed origin this pattern becomes more weak. In under-expanded regime (Fig. 7b) the correlation map is characterized by a pattern

with a spatial phase shift of approximately 0.25 D (half of the previous one evaluated for the incompressible regime). Downstream from the fixed point, the intensity of the peaks of the correlation map in under-expanded regime increases up to 48% of the values of the peaks detected for M=0.3. This is due to the presence of the shock-cells structures in the potential core. For both cases, the peaks are located along the jet axis and their intensity decreases moving downstream from the fixed point. This reduction with respect to the centreline coordinate is not monotonic for the under-expanded regime.

In Fig. 7, the axial extent of the transverse correlation decreases from nearly 1 D for M=0.3 to 0.25 D for M=1.1. The correlation map is stretched and compressed along two different principal directions. These directions are aligned with the axial and radial ones and delimit four quadrants of negative correlation levels.

In Fig. 8, the longitudinal correlations, valuated at r/D=0.5 (in the shear layer region) and x/D=2 for Mach numbers M=0.3 and 1.1, are shown. The inclined nature of the pattern of the correlation map with respect to the axis of the jet is detected. This feature is due to the straining of the large-scale turbulence structures as shown by [18-19-20]. Fleury [19] pointed out that such inclination is attributed to the turbulence anisotropy induced by the mean shear flow. The size of the longitudinal correlations in underexpanded regime (Fig. 9b) is slightly reduced compared with its extension in incompressible regime (Fig. 9a), in particular the compressibility effects alter the turbulent structures inducing a wide variety of scales in the shear layer as shown by [13].

The longitudinal correlations map valuated at r/D=0 and x/D=8 for Mach numbers M=0.3 and 1.1 are shown in Fig. 10a and 10b, respectively. Downstream from the end of the potential core, the correlation function is stretched along the longitudinal direction. In Fig. 11, the correlation functions are inclined with respect to the axial direction. In particular, in Fig. 10b the correlation function is elongated upstream from the origin.

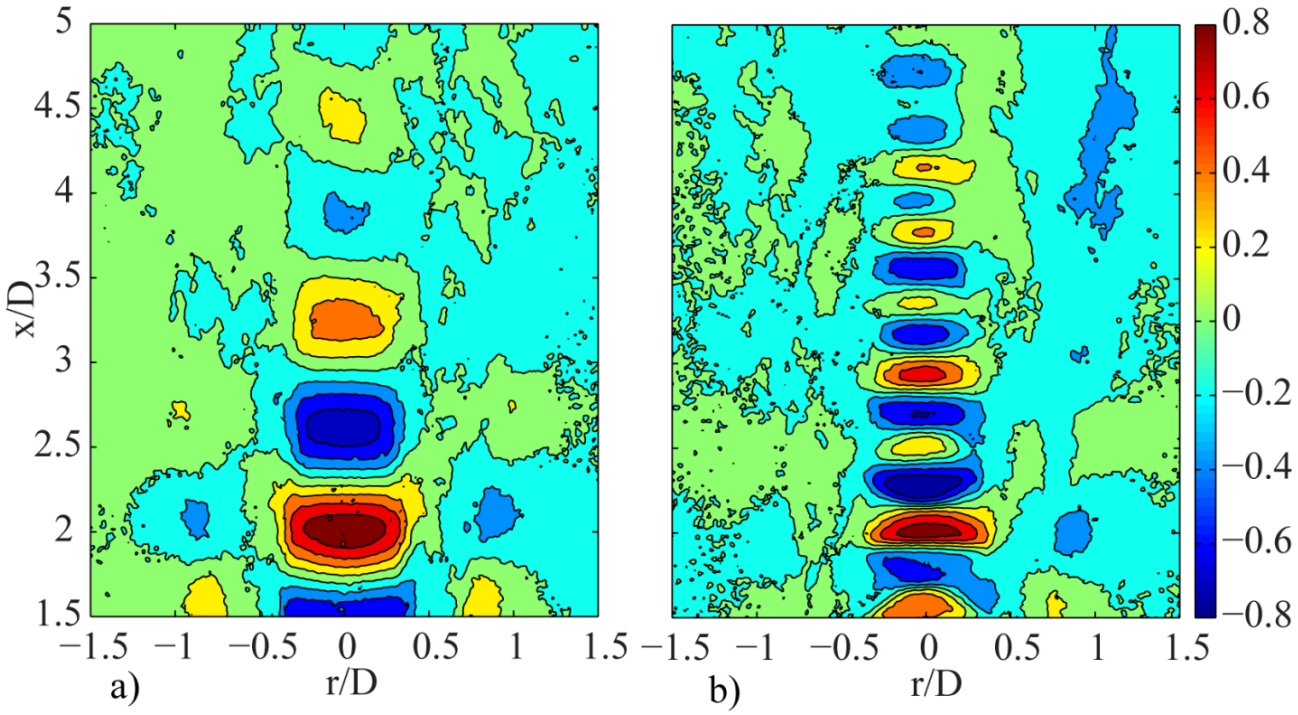

Figure 7 Normalized distribution of two-point correlation of the axial turbulent intensity at r/D=0 and x/D=2 for Mach numbers (a) M=0.3 and (b) 1.1.

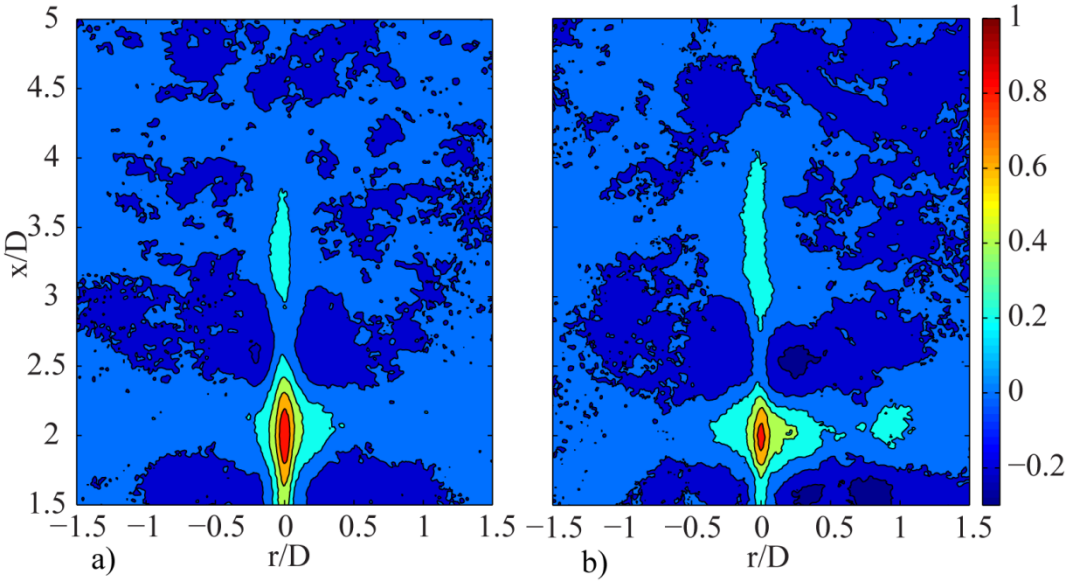

Figure 8 Normalized distribution of two-point correlation of the radial turbulent intensity at r/D=0 and x/D=2 for Mach numbers (a) M=0.3 and (b) 1.1.

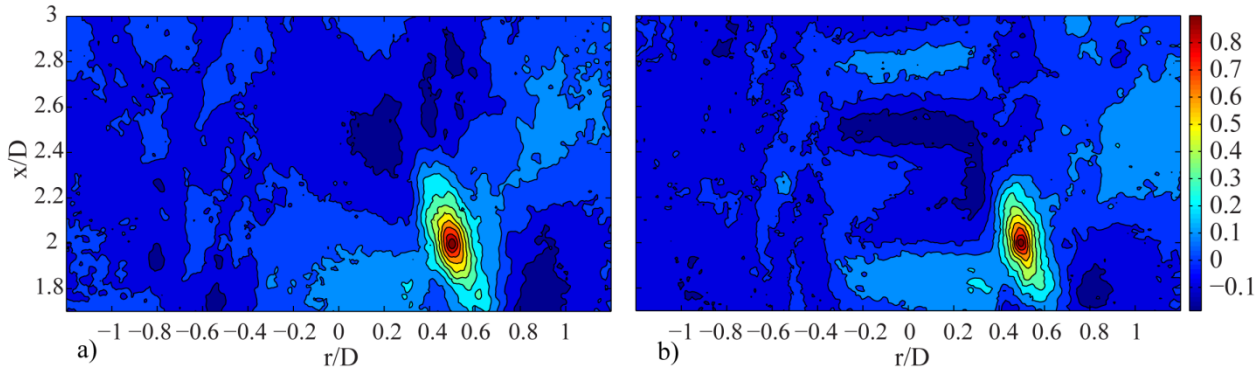

Figure 9 Normalized distribution of two-point correlation of the axial turbulent intensity at r/D=0.5 and x/D=2 for Mach numbers (a) M=0.3 and (b) 1.1.

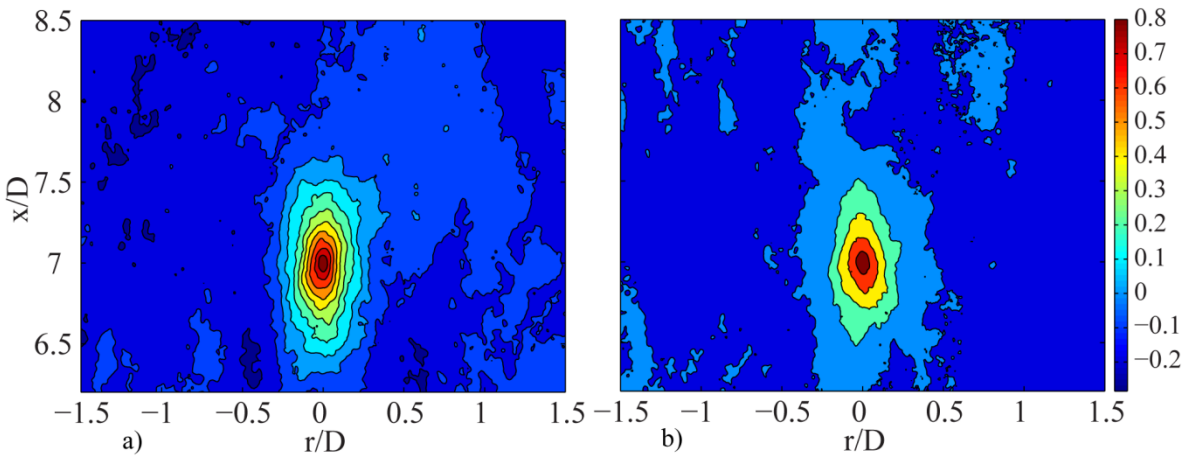

Figure 10 Normalized distribution of two-point correlation of the axial turbulent intensity at r/D=0 and x/D=7 for Mach numbers (a) M=0.3 and (b) 1.1.

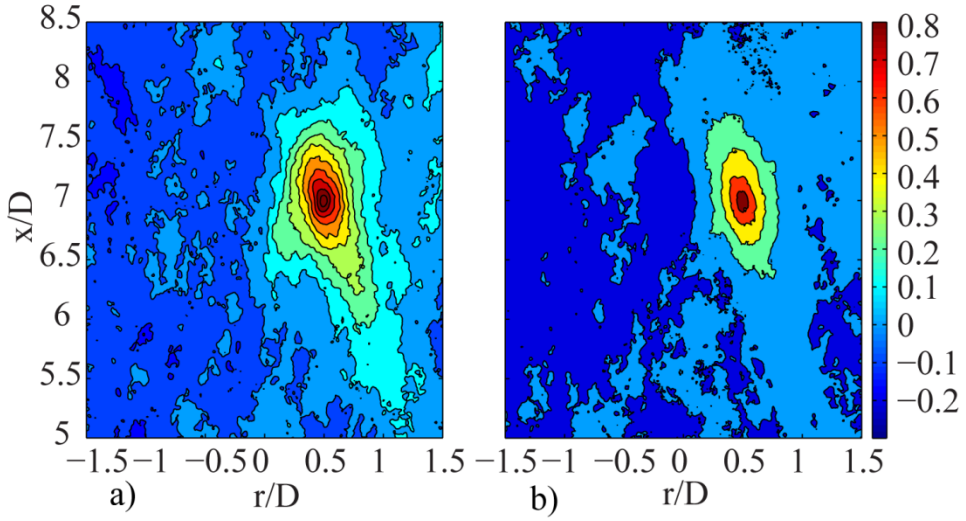

Figure 11 Normalized distribution of two-point correlation of the axial turbulent intensity at r/D=0.5 and x/D=7 for Mach numbers (a) M=0.3 and (b) 1.1.

CONCLUSIONS

The compressibility effects are investigated in terms of turbulent statistics in order to characterize the near field of high-speed turbulent jet operated at high Reynolds number at Mach numbers M=0.3, 0.9 and 1.1 (under-expanded regime). The analysis comprises flow field measurements using high spatial resolution planar PIV experiments. In order to characterize the basic flow field, the single-point statistics are presented and compared with previous works [19-20-24-25]. In under-expanded regime, the spatial evolution of the jet reveals the presence of shock-cell structures into the potential core region that extend up to 4.5 D downstream from the nozzle exit.

Two-point statistics have been presented in order to investigate the large spatial coherent structures in the potential core and the shear layer regions. The distribution of the longitudinal spatial correlations valuated in the potential core region of the jet exhibits a phase shifted pattern in sign that extends periodically along the jet axis. This spatial phase shift is approximately 0.5 D for M=0.3 and 0.25 D for M=1.1. This change can be due to the interaction of the shock-cell structures that arise in under-expanded regime.

ACKNOWLEGMENTS

This research has been conducted as part of the ORINOCO project funded by the European Community's Seventh Framework Program (FP7-AAT-2010-RTD-Russia; project number 266103).

REFERENCES

[1] Hussain AKMF and Clark AR "On the coherent structure of the axisymmetric mixing layer: a flow-visualization study" J. Fluid Mech 104 (1981) pp. 263-294.

[2] Pope BS "Turbulent Flows" Cambridge University Press (2000).

[3] Crow SC and Champagne FH "Orderly structure in jet turbulence" J. Fluid Mech. 48 (1971) pp. 547-591.

[4] Yule AJ "Large-scale structure in the mixing layer of a round jet" J. Fluid Mech. 89 (1978) pp. 413-432.

[5] Hussain F "Coherent structures and turbulence" J. Fluid Mech. 173 (1986) pp. 303-356.

[6] Zaman K and Hussain F "Turbulent Shear Flow" Pennsylvania State University (1977) pp. 11-23.

[7] Liepmann D and Gharib M "The role of streamwise vorticity in the near-field entrainment of round jets" J. Fluid Mech. 245 (1992) pp. 643-643.

[8] Raffel M, Willert CE and Kompenhans J “Particle image velocimetry: a practical guide” Springer Verlag, 1998.

[9] Brown GL and Roshko A “On density effects and large structure in turbulent mixing layers” J. Fluid Mech. 64 (1974) pp. 775-816.

[11] Fourguette DC, Mungal MG and Dibble RW “Time evolution of the shear layer of a supersonic axisymmetric jet" AIAA journal 29 (1991) pp. 1123-1130.

[10] Papamoschou D and Roshko A “The compressible turbulent shear layer: an experimental study” J. Fluid Mech. 197 (1988) pp. 453-477.

[12] Murakami E and Papamoschou D “Eddy convection in coaxial supersonic jets” AIAA journal 38 (2000) pp. 628-635.

[13] Thurow B, Samimy M and Lempert W “Compressibility effects on turbulence structures of axisymmetric mixing layers” Ph. of Fluid. 15 (2003) pp. 1755-1765.

[14] Hileman J, Thurow BS, Caraballo EJ and Samimy M “Large-scale structure evolution and sound emission in high-speed jets: real-time visualization with simultaneous acoustic measurements” J. Fluid Mech. 544 (2005) pp. 277–307.

[15] Lumley JL “The structure of inhomogeneous turbulent flows” Atmospheric turbulence and radio wave propagation (1967) pp. 166-178.

[16]Seiner JM, Ukeiley L and Ponton MK “Jet noise source measurements using PIV” AIAA/CEAS Aeroacoustics Conference and Exhibit, 5th, Bellevue, WA. (1999).

[17] Lighthill MJ “On sound generated aerodynamically. I. General theory” Proceedings of the Royal Society of London. Series A. Mathematical and Physical Sciences 211 (1952) pp. 564-587.

[18] Ukeiley L, Tinney C, Mann R and Glauser M “Spatial correlations in a transonic jet” AIAA journal 45 (2007) pp. 1357-1369.

[19] Fleury V, Bailly C, Jondeau E, Michard M and Juvé D “Space-time correlations in two subsonic jets using dual particle image velocimetry measurements” AIAA journal 46 (2008) pp. 2498-2509.

[20] Arakeri VH, Krothapalli A, Siddavaram V, Alkislar MB and Lourenco LM “On the use of microjets to suppress turbulence in a Mach 0.9 axisymmetric jet” J. Fluid Mech. 490 (2003) pp. 75-98.

[21] Kerhervé F, Jordan P, Gervais Y, Valiere JC and Braud P “Two-point laser Doppler velocimetry measurements in a Mach 1.2 cold supersonic jet for statistical aeroacoustic source model” Exp. Fluids 37 (2004) pp. 419-437.

[22] Abramovich GN, Girshovich TA, Krasheninnikov SI, Sekundov AN and Smirnova IP “The theory of turbulent jets” Moscow Izdatel Nauka (1984).

[23] Violato D “3D flow organization and dynamics in subsonic jets - aeroacoustic source analysis by tomographic PIV” PhD thesis Delft University of Technology (2013).

[24] Tinney CE, Glauser MN and Ukeiley LS “Low-dimensional characteristics of a transonic jet. Part 1. Proper orthogonal decomposition” J. Fluid Mech. 612 (2008) pp. 107-141.

[25] Alkislar MB, Krothapalli A and Butler GW “The effect of streamwise vortices on the aeroacoustics of a Mach 0.9 jet” J Fluid Mech. 578 (2007) pp. 139-169.